Environmental Modelling and Software 183 (2025) 106228

Contents lists available at ScienceDirect

Environmental Modelling and Software

journal homepage: www.elsevier.com/locate/envsoft

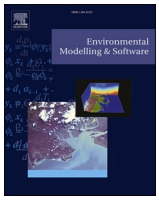

An operational IoT-based slope stability forecast using a digital twin

Luca Piciullo *, Minu Treesa Abraham, Ida Norderhaug Drøsdal, Erling Singstad Paulsen

Norwegian Geotechnical Institute (NGI), Oslo, Norway

ARTICLE INFO

Keywords:
Real-time monitoring
Modelling
Landslides
Early warning
Machine learning

ABSTRACT

The paper investigates the combined use of real-time hydrological monitoring, publicly available meteorological data and hydrological and geotechnical numerical modelling, to develop data-driven models to forecast the stability of a slope. This study showcases a first attempt to integrate these critical aspects into a fully automatic Internet of Thing (IoT)-based local landslide early warning system (Lo-LEWS).

The paper uses a validated hydrological numerical model, back-calculated over real monitored conditions, to evaluate the slope stability. The factor of safety (*FoS*) was computed coupling the commercial package GeoStudio, using transient SEEP/W and Slope. The analyses were conducted for 5 different 1-year datasets encompassing both historical (2019–2020, 2021–2022, 2022–2023) and future projections (2064–2065, 2095–2096) of meteorological variables. Daily variation of hydrological and meteorological variables, along with vegetation indicators were used as inputs to train data-driven models, using polynomial regression (PR) and Random Forest (RF), to forecast daily *FoS* values. The trained models proved to be effective and were employed to forecast slope stability for the rolling three days. To accurately forecast the *FoS*, it was essential to incorporate forecasted hydrological, meteorological and vegetation variables into the analysis. The hydrological variables used as inputs for the data-driven models are forecasted using an open-source Python package for the analysis of hydrogeological time series, called Pastas (Collenteur et al., 2019). This model uses historical and forecasted meteorological and vegetation conditions to, specifically, replicate and forecast the time series of volumetric water content (VWC) and pore water pressure (PWP). The forecasted hydrological variables from Pastas, the forecasted meteorological variables as well as Leaf Area Index (*LAI*) are used as inputs for the trained data-driven models to forecast the *FoS* values.

Finally, a web-based platform (WBP) has been created that automatically runs once a day and perform the following actions: 1) fetches measured and forecasted data using APIs, 2) runs rolling three days forecast based on collected hydrological, meteorological and vegetation variables, and 3) sends the forecasted values back to the Norwegian Geotechnical Institute (NGI) data platform, NGI Live, making them available for real-time visualization in online dashboards. If *FoS*, VWC or PWP threshold values are exceeded, text messages and emails are sent to the system managers, enabling them to take appropriate actions. The successful implementation of this framework is the result of a collaborative effort across diverse expertise areas, including geotechnics, hydrology, meteorology, instrumentation, and informatics.

1. Introduction

The advancement in slope instrumentation technology and the consequent cost reductions, have made it possible to build low-cost monitoring networks, linking the different sensors and providing real-time monitoring data. Monitoring is an essential component, but not sufficient, to forecast the occurrence of landslides (Dibiagio and Kjekstad, 2007; Bell, 2010; Intrieri et al., 2013; Calvello et al., 2015; Fathani et al., 2016; Calvello, 2017; Piciullo et al., 2018). A reliable model (such as physically-based, numerical, empirical, probabilistic) should be defined to establish a connection between the data collected through monitoring— encompassing variables like precipitation, soil moisture, and ground displacement—and the potential occurrence of landslides. In addition, the model is important during the forecasting phase, where, considering weather forecasts, it evaluates the stability of the slope. Moreover, different warning conditions based on the model's outputs

* Corresponding author.
E-mail addresses: luca.piciullo@ngi.no (L. Piciullo), minu.treesa.abraham@ngi.no (M.T. Abraham), ida.norderhaug.drosdal@ngi.no (I.N. Drøsdal), erling.singstad.paulsen@ngi.no (E.S. Paulsen).

https://doi.org/10.1016/j.envsoft.2024.106228
Received 13 March 2024; Received in revised form 2 September 2024; Accepted 24 September 2024
Available online 5 October 2024

need to be defined. Monitoring, modelling, forecasting and warning are the main technical components for the effective operation of a landslide early warning system-LEWS (Piciullo et al., 2018).

LEWS can be employed at two different scales of analysis (Thiebes et al., 2012; Calvello et al., 2015; Stähli et al., 2015; Thiebes and Glade, 2016; Piciullo et al., 2018): slope and regional. The systems employed at a slope scale can be named as "local" (Lo-LEWS, Piciullo et al., 2018). They refer to the monitoring and forecasting of a landslide at a slope unit, where usually, a sliding surface can be identified. On the other hand, systems employed at regional scale can be referred as "territorial" (Te-LEWS (Piciullo et al., 2018), or "geographical" (Guzzetti et al., 2020), indicating that the system aims at forecasting the occurrence of many landslides in a large area, such as a municipality, province, region or even a nation. Pecoraro et al., 2019 highlights that for 28 out of 29 reviewed Lo-LEWS, the main variable used to issue a warning is the velocity of the displacement. This is particularly true when dealing with landslides that have already shown deformations. However, challenges arise when dealing with slopes that have not shown any prior displacements but that are still potentially dangerous for the presence of elements exposed, such as people, structures, and infrastructures in the potential runout area.

This paper proposes an operational Internet of Things (IoT)-based slope stability forecast grounded on hydrological and weather monitoring variables for a steep slope, that has not shown any prior deformation. IoT in the context of landslide warning can be described as the use of various sensors, strategically placed in the landslide prone areas, to continuously collect data and transmit them in real-time for interpretation and analysis. This information can be used to automatically inform relevant authorities, first responders, and local communities to take appropriate measures to mitigate potential consequences. Currently, in literature, there are not so many contributions proposing an operational real-time slope stability forecast for Lo-LEWS purposes and among the available, most deal with displacement measurements for slow moving landslides. El Houssaini et al., 2022 propose a prototype LEWS based on a network of wireless sensor nodes and an ultra-wideband (UWB) for distance measurements in real-time of slow-moving (cm/s) surface slide. Charléty et al., 2023, employ Radio-Frequency Identification (RFID) tags to monitor landslide surface displacement, this method is applied for slow displacements lower than 1 cm per day. Ju et al., 2015, present a real-time monitoring and warning based on velocity displacements measured with inclinometers. Abraham et al., 2020; Gamperl et al., 2021, propose the use of low-cost micro-electro-mechanical systems-based tilt sensors and water sensors for the detection of ground movements and water content measurement. Similar displacements-based approaches are used by Kotta et al., 2011; Sofwan et al., 2017; Park et al., 2019; Sun et al., 2024, among others. In the context of fast-moving rainfall-induced landslides, the existing literature is limited in its coverage of real-time hydrological and rainfall monitoring, particularly at a regional scale. Recent papers addressing real-time monitoring phase include those by Gian et al., 2017, Mirus et al., 2018, Kim et al., 2021, Kuradusenge et al., 2021, Oguz et al., 2022; Marino et al., 2023. There is a notable gap in attention given to the IoT-based modelling and forecasting phases. Additionally, crucial variables such as pore water pressure and meteorological factors like relative humidity, solar radiation, and temperature are often overlooked, even though these variables are critical in determining the hydrological behaviour and influencing the stability of the slope. However, it is difficult to consider their effects into account without a process-based model. One challenge in the use of physically based or process-based models for real-time slope stability analysis lies in the difficult integration of such models into a cloud-based service. As a result, there is a need for further research and development to bridge this gap and enhance the forecast of rainfall-induced landslides. The alternative option, as adopted in literature, is the use of thresholds based on triggering factors such as rainfall or field-based displacement measurements or a combination of both (Abraham et al., 2022). However, this approach completely ignores the underlying physics that triggers slope instabilities, relying entirely upon the measured data and their historic relationship with landslides at a given location. This study addresses this challenge using data-driven models. These models use a dataset that includes inputs from field-based hydrological monitoring, meteorological conditions, and vegetation data, along with factor of safety (*FoS*) values derived from a numerical model.

This study represents a first attempt of a real-time slope stability forecast considering different hydrological, meteorological and vegetation variables for a non-failed steep slope. The 4-phase framework for Lo-LEWS (Piciullo et al., 2022) based on: monitoring, modelling, forecasting, warning; has been implemented. The monitoring and modelling set up are presented in detail in Piciullo et al., 2022, using an unsaturated slope in Norway as pilot case study. This paper covers the outcomes of the digital twin of the slope, the forecasts of the hydrological variables, the application of data-driven models for forecasting the *FoS*. Finally, it provides a comprehensive overview of the operational structure of the IoT based digital twin.

2. Study area and in situ real-time monitoring: a summary

The study area is in Eidsvoll municipality, Akershus County, Norway (60° 19′ 23.376″, 11° 14′ 44.646″). The climate in Eidsvoll is characterized by moderate rainfall, low humidity, minimal wind, and significant daily and annual temperature fluctuations. However, the region has experienced frequent and prolonged rainfall events. For instance, in the autumn of 2000, several landslides were triggered by nearly three months of continuous rainfall (Jaedicke and Kleven, 2008). High cumulative rainfall has been also registered in the summer of 2011, when floods and landslides occurred. In the study area, the Precambrian Granodioritic to Tonalitic gneiss forms the bedrock underneath the Quaternary deposits (clay, sand and gravel). Due to the presence of Vorma river, glacifluvial and fluvial sand and gravel deposits cover various locations in Eidsvoll.

The monitored slope is approximately 25 m high, with an inclination of about 45° in the upper part. The slope has not shown any prior deformations, but it is a threat for the railway lines located at the toe. Additionally, the slope is situated immediately to the east of a cultural heritage site that includes a 12th-century church and its graveyard. This proximity makes it impossible to implement structural slope stability measures directly on the slope. Consequently, the slope has been equipped with several sensors. According to the classification of Hungr et al., 2014; Cruden and Varnes, 1996, the possible expected landslide phenomena could be classified as rapid to very rapid, silt slide that can evolve in a flowslide. In late spring/early summer of 2016, SM150T[6] volumetric water content (VWC) and soil temperature sensors, along with GEOTECH PVT[7] piezometers for measuring pore-water pressure (PWP), were installed to monitor the hydrological conditions within the slope (blue triangles and rectangles in Fig. 1). The SM150T[6] VWC capacitance sensors were positioned on top of the slope (Fig. 1), at six different depths: 0.1 m, 0.5 m, 1 m, 2 m, 4 m, and 6 m (blue rectangles in Fig. 2). GEOTECH PVT[7] electronic piezometers with logging memory were installed at four different depths: 6 m, 9 m, 15 m, and 23 m (blue triangles in Figs. 1 and 2).

In May 2021, three TEROS-12[3] soil water content, and three TEROS-21[4] water potential sensors were installed on the slope at approximately 163 m a.s.l., at depths 0.1 m, 0.5 and 0.9 m (green rectangles and circles in Figs. 1 and 2). In June 2022, an ATMOS-41[2] weather station was installed at the top on the slope (grey square in Figs. 1 and 2). Additionally, a TEROS-12[3] and a TEROS-21[4] were installed at circa 167 m a.s.l. (yellow square and circle in Figs. 1 and 2).

The components of the installed real-time sensor systems and the variables measured are outlined in Table 1. The sensors and weather station regularly send data to a data platform, which stores the measured values and provides both dashboards and an Application Programming Interface (API) to access the data in real-time.

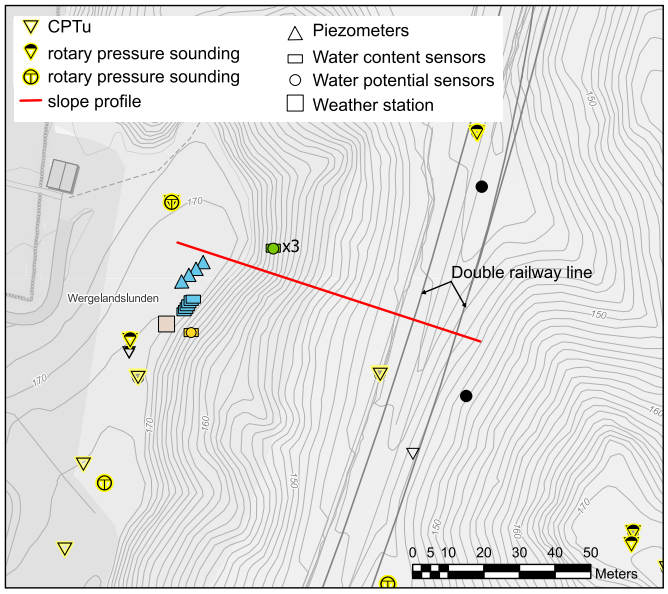

Fig. 1. Plan view with 1 m contour lines, location of geotechnical field investigations, monitoring sensors, slope profile considered for the GeoStudio model (Piciullo et al., 2022) and railway lines.

Lab testing (granulometric curves, pressure plate tests, Atterberg limits) and in-situ CPTu tests (Fig. 1) have been carried out (Heyerdahl et al., 2018). The slope has been discretized in the following layering: a sandy silt layer of around 6 m depth, a smaller layer of clayey silt material (about 3 m thick), and a firm marine clay layer to large depths (Fig. 2).

As stated earlier, the weather station and some of the soil VWC and water potential (WP) sensors were installed recently, and the data were not available for the dataset time frames considered in this study. Therefore, the measurements from the six SM150T VWC[6] sensors and the PWP sensor at 6 m depth, which were installed in 2016, are the ones considered in this study. The soil beneath 7 m is in saturated condition, thus the piezometers installed at deeper depths were neglected (Piciullo et al., 2022). From here on in this article, the abbreviation VWC represents the volumetric water content at all the six depths considered (0.1 m, 0.5 m, 1 m, 2 m, 4 m and 6 m), and PWP represent the pore-water pressure at 6 m.

3. Methodological approach

3.1. IoT-based system structure

This study integrates the digital twin framework proposed by Piciullo et al., 2022, for rainfall-induced landslide at slope scale, into an operational real-time IoT-based system designed for early warning purposes. The architecture of the system includes the 4-phase technical aspects of monitoring, modelling, forecasting and warning (Fig. 3).

In the monitoring phase, sensors from different companies are used to monitor meteorological and hydrological variables. The data are collected from the different cloud-based sources and are stored and made available using NGI live (Fig. 3). NGI Live is a web-based platform (WBP) where the user can analyse the data gathered from different sources in real-time. Such platforms are becoming a fundamental non-structural disaster mitigation measure, due to their role in real-time monitoring and early warning (Bossi et al., 2023). The digital twin is set up as a cloud service, regularly forecasting slope stability using hydrological and meteorological data. The cloud service runs once a day, fetching data from NGI Live, the Norwegian Meteorological Institute (MET Norway) and, Open-meteo through APIs. It runs the digital twin and publishes the results to NGI Live. NGI live and the digital twin of the slope under investigation belong to the modelling phase.

Azure Functions [8] are used to deploy the cloud service. Azure Functions is a serverless solution provided by Azure to simplify creating cloud services. It provides a set of event-driven triggers and bindings to run code and to connect it to other services. The service is deployed as an Azure Function with a Timer Trigger [9] which runs a python function containing the forecast code (i.e., the digital twin) every day at midnight local time (Europe/Oslo).

The execution of the cloud service can be monitored through Azure Monitor [10]. Pre-trained models and other data needed by the analysis are stored in Azure Blob Storage [11] and secrets (e.g. client credentials for the APIs) are stored in Azure Key Vault [12]. Finally, the forecasted data are visualized in real-time, in the online dashboards (the link to video examples is available in the section Software and data availability) set up in NGI Live (Fig. 3). If the forecasted hydrological variables (i.e., VWC and PWP) or *FoS* exceed some pre-defined threshold values, then, warning messages and emails are sent to system managers.

3.2. The digital twin

In the context of slope stability, a digital twin can be seen as a reliable virtual model of a real slope, created to simulate, analyse, and predict the behaviour of the slope under various conditions. This digital replica

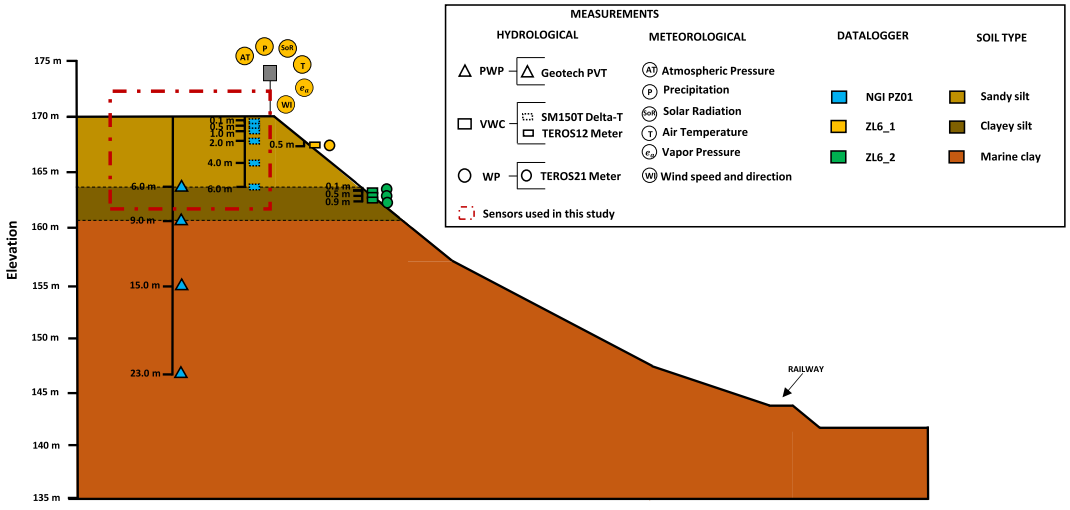

Fig. 2. Schematization of the studied slope, with soil stratigraphy and location of the sensors.

Table 1
Components of the installed sensors and the measured variables. References in square brackets refer to the webpage reference list.

Sensor name	Variables measured	Measurement Interval	Data logger and provider
ATMOS-41 [2]	Solar radiation Precipitation Relative humidity Air temperature Humidity sensor temperature Vapor pressure Barometric pressure Horizontal wind speed Wind gust Wind direction Tilt Lightning strike count Lightning average distance	5 min	ZL6 Data Logger, Meter Group [1]
TEROS12 Meter [3]	Volumetric water content Soil temperature Electrical conductivity	1 h	ZL6 Data Logger, Meter Group [1]
TEROS21 Meter [4]	Water potential Soil temperature Electrical conductivity	1 h	ZL6 Data Logger, Meter Group [1]
SM150T Delta-T [6]	Volumetric water content Soil temperature	1 h	GP2 Data Logger, Delta-T Devices [5]
Geotech PVT [7]	Pore pressure	1 h	NGI PZ01 Data Logger, NGI

integrates geotechnical, environmental, and hydrological information with data from multiple sources, including field surveys, monitoring data, and meteorological conditions, to provide a comprehensive and dynamic representation of the slope.

The numerical model described in Piciullo et al., 2022, trained data-driven models (described in Section 4), along with Pastas (Collenteur et al., 2019; described in Section 5) have been used to build a digital twin of the slope under investigation, allowing for real-time simulations (Fig. 4) using the meteorological and hydrological data. Historical and forecasted meteorological data are used as inputs into a python-based package called Pastas to forecast the hydrological variables, VWC and PWP for the rolling three days. The forecasted VWC and PWP values, along with forecasts of climate and vegetation variables are used as inputs for data-driven models to forecast the *FoS*.

A flowchart that outlines the explanatory variables employed for forecasting hydrological variables (VWC and PWP) and *FoS* values is shown in Fig. 4. The chart also includes a timeline to enhance the understanding of the chronological sequence involved in the forecasting process. The VWC and PWP values are modelled using both historical measurements and forecasts of precipitation (*P*), air temperature (*T*), snow depth (*SD*), relative humidity (*RH*), wind speed (*WS*), solar radiation (*SoR*), albedo (Fig. 4). The historical data are fetched for the past rolling 365 days during every run and the future data, for the rolling three days. Historical and forecasted data are retrieved from MET Norway and Open-meteo (Fig. 4), specifically, from Frost API [13] (references in square brackets refer to the webpage reference list), Historical weather API [14], Locationforecast API [15] and Weather forecast MET Norway API [16]. The historical data from the Norwegian Meteorological Institute are collected from weather stations, while the data from open-meteo is grid-based. The weather data together with *SoR*, *LAI*, and Albedo, modelled as cyclic functions, are used as inputs in Pastas to forecast the hydrological variables. Pastas, thus, forecasts the hydrological variables VWC and PWP for the upcoming 72 h (i.e. rolling three days), utilizing historical data and meteorological forecasts. The forecasted hydrological variables, along with *T*, and the *LAI* are the inputs of the pre-trained data-driven models for the *FoS* forecast of the rolling 3 days. The duration of 72 h is chosen arbitrarily as a suitable time interval for early warning purposes.

4. Data-driven machine learning models definition

4.1. Datasets definition

A validated numerical model of the slope has been defined in Piciullo et al. (2022). The model has been used to compute the *FoS* using five different 1-year period datasets: 3 belonging to the past and 2 to the future. The datasets are starting the same day of the year, i.e., June 1. The time-dependent input variables used in GeoStudio, transient SEEP analysis coupled with Slope, are grouped into meteorological and

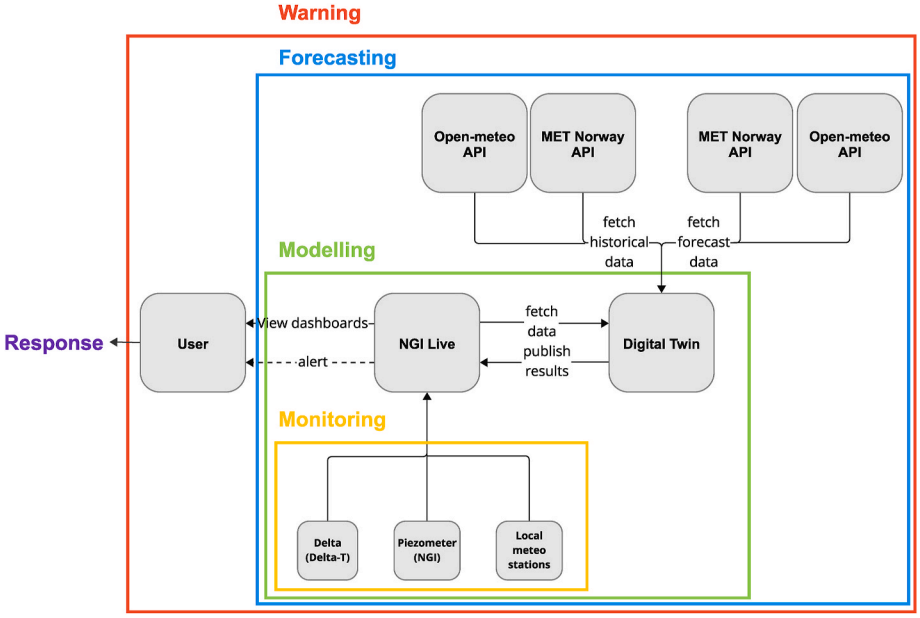

Fig. 3. IoT-based system for early warning purposes: the operational architecture.

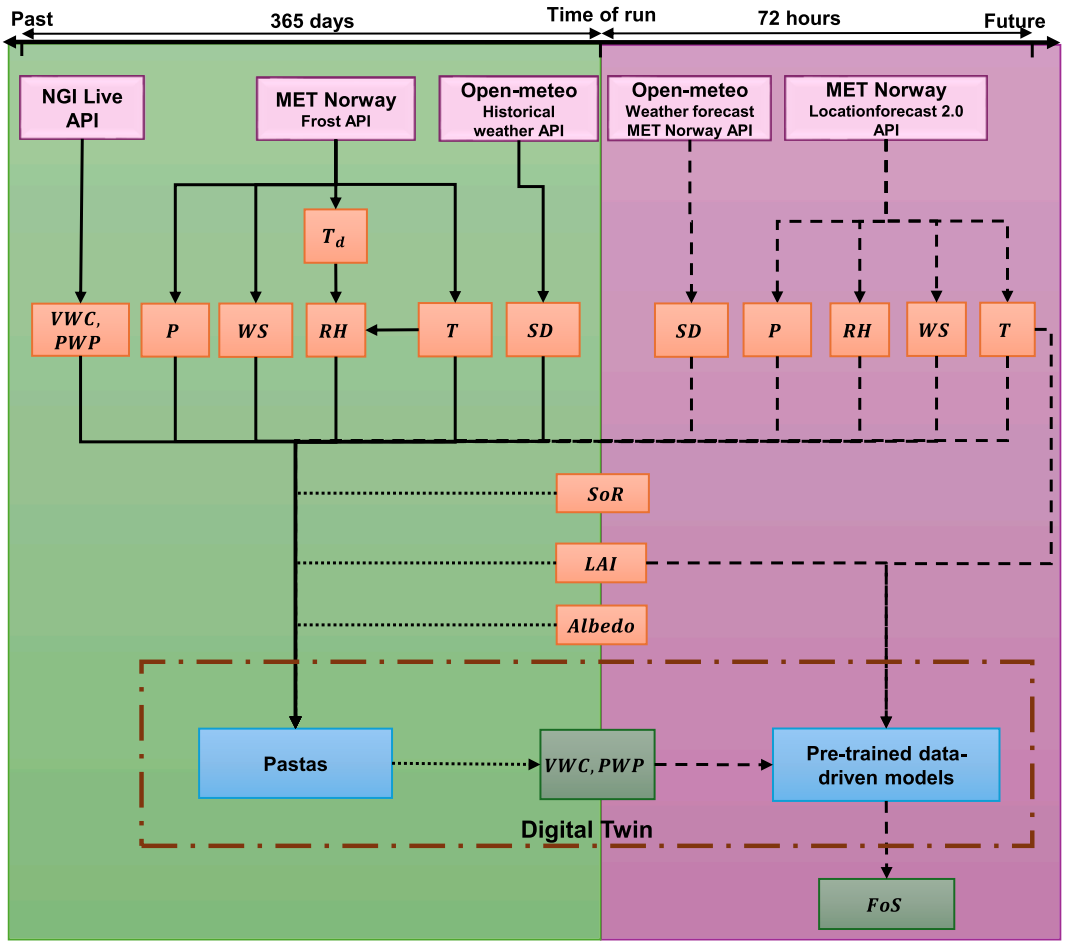

Fig. 4. Flowchart showing the variables used for forecasting VWC, PWP and *FoS*. The firm lines indicate inputs from past and the dashed lines indicate inputs from future. The dotted lines indicate that the variable has values from both past and future.

vegetation (Table 2). They are: *P*, *T*, *SD*, *RH*, *WS*, *SoR*, albedo, *LAI*, root depth (*RD*), and vegetation height (*VH*). It is worth mentioning that *P* refers to rainfall plus snowfall, and *SD* have been considered as an input. This approach differs from Piciullo et al. (2022), where *P* refers to rainfall and snowmelt. The change was made because it is easier to collect forecasted values for snowfall rather than snowmelt.

The input data for the physics-based model have been collected from various sources based on availability (Table 2). Past 1-year daily *P*, *T* and *SD* datasets have been retrieved from the daily gridded raster file of SeNorge [17]. SeNorge provides high-resolution 1 km grid of daily data for applications requiring long-term datasets (Lussana et al., 2018). For the future scenarios, *P* and *T* datasets have been obtained from the Norwegian Centre for Climate Services (Norsk klimaservicesenter, [18]), while *SD* has been neglected. The centre is established by a collaboration between the Meteorological Institute, the Norwegian Water Resources and Energy Directorate, the Mapping Authority, NORCE and the Bjerknes Center. The aim is to disseminate meteorological and hydrological data to be used for climate adaptation and

Table 2
Hydrological, meteorological and vegetation variables for the past and future datasets.

	Past datasets			Future datasets	
	2019–2020	2021–2022	2022–2023	2064–2065	2095–2096
Hydrological variables					
VWC	sensors (NGI Live)	sensors (NGI Live)	VWC (NGI Live)	Modelled values from GeoStudio	Modelled values from GeoStudio
PWP	Piezometer (NGI Live)	Piezometer (NGI Live)	Piezometer (NGI Live)	Modelled values from GeoStudio	Modelled values from GeoStudio
Meteorological variables					
P	Senorge	Senorge	Senorge	Norsk klimaservicesenter	Norsk klimaservicesenter
T	Senorge	Senorge	Senorge	Norsk klimaservicesenter	Norsk klimaservicesenter
SD	Senorge	Senorge	Senorge	*none*	*none*
RH	Oslo station	Gardemoen station	Gardemoen station	Oslo station (2019–2020)	Oslo station (2019–2020)
WS	Oslo station	Gardermoen station	Gardermoen station	Oslo station (2019–2020)	Oslo station (2019–2020)
SoR	Sinusoidal function	Sinusoidal function	Sinusoidal function	Sinusoidal function (2019–2020)	Sinusoidal function (2019–2020)
Albedo	Cherubini et al. (2017)	Cherubini et al. (2017)	Cherubini et al. (2017)	Cherubini et al. (2017)	Cherubini et al. (2017)
Vegetation variables					
LAI	Rectangular function	Rectangular function	Rectangular function	Rectangular function	Rectangular function
RD	Constant	Constant	Constant	Constant	Constant
VH	Constant	Constant	Constant	Constant	Constant

further research on the impact of climate change on nature and society. The forecasts came from ten regional climate projections obtained from Euro-CORDEX. The *P* and *T* data were downloaded for two 1-year periods in the future: 2064–2065 and 2095–2096. The regional climate projections used was Swedish Meteorological and Hydrological Institute (CNRM_RCA), based on a Representative Concentration Pathways (RCP) of 8.5, representing a high greenhouse gas emission scenario. This model was selected because it gives the expected annual rainfall amount for the case study location, considering an annual rainfall increase of 15% due to climate change (Hanssen-Bauer et al., n.d.), specifically, 1235 mm for 2064–2065 and 1295 mm for 2095–2096. The data were retrieved using a python code for the selected case study area. *RH* and *WS* data have been collected from either Gardermoen station (closer to the test site), if available, or from the Oslo meteorological station (Table 2). The trends and values, measured at the two stations, have been compared for 1 year period showing a good agreement ($R^2 = 0.6$) for *WS* and ($R^2 = 0.84$) for *RH*. The *SoR* has been considered as a sinusoidal function estimated for the case study location, using GeoStudio. To be used as future dataset, the *SoR* values for the years 2019–2020 obtained using GeoStudio was fitted using a sinusoidal model (Eq. (1), as a function of the day of the year.

$$f(x) = a.\sin(b.(x-c)) + d \quad (1)$$

where *a* is the amplitude of the sine wave, representing the maximum value of solar radiation, *b* is the frequency of the sine wave, related to the period of the cyclic variation, *c* is the phase shift, indicating the horizontal shift of the wave along the *x*-axis and *d* is the vertical shift, representing the baseline value of solar radiation. The initial estimates for the sinusoidal parameters (amplitude, frequency, phase, and offset) are defined based on the characteristics of the *SoR* data modelled using GeoStudio. Albedo input data has been derived from Cherubini et al., 2017. *LAI* has been represented with a rectangular function (Table 2) having a maximum of 1.5 in plant growing seasons and 0 in winter months (Dahlberg et al., 2004; Capobianco et al., 2021). *RD* and *VH* are set as constants and equal, 1 m and 3 m respectively (Table 2). Furthermore, when considering future scenario datasets for the *FoS* calculation, it is noteworthy that the inputs have been arbitrarily chosen to be identical to those of the 2019–2020 period, except for *P* and *T*, which are assessed using forecasting meteorological models (Table 2). This approach aims to maintain consistency while accounting for variations in climatic factors.

The meteorological and vegetation variables for the five 1-year datasets (see Table 2) have been used as inputs in the validated GeoStudio model of the slope (for details see Piciullo et al., 2022) to calculate the *FoS*. The sliding surface considered in the calculations is the same for the different datasets and it lies in the upper steepest part of the slope. The sliding surface selected was the one showing the lowest values of the *FoS* in time for all five datasets. The *FoS* trends for the five 1-year datasets exhibits a similar pattern (Fig. 5). The *FoS* values tend to increase during summer months, reaching peak values likely due to the presence of vegetation with high values of *LAI* and *VH*, as well as high air temperature that generates significant suction in the unsaturated soil. In contrast, the *FoS* values decrease during the autumn months and remain low throughout winter and spring. This is due to increased pore water pressure caused by higher infiltration rates from rainfall, snowmelt and the absence of leaves.

4.2. Data-driven models for slope stability forecast

The next step involved the training of the data-driven models to forecast the *FoS* by incorporating different predictor variables. This is achieved with the aim of defining relationship between *FoS* and meteorological, hydrological and vegetation variables. Different data-driven methods were considered for the forecast, such as: Linear regression, Polynomial regression, Random Forest, Bayesian Ridge, Multilayer perceptron. The best two, i.e., Polynomial regression (PR), Random Forest (RF) are described in detail in the following.

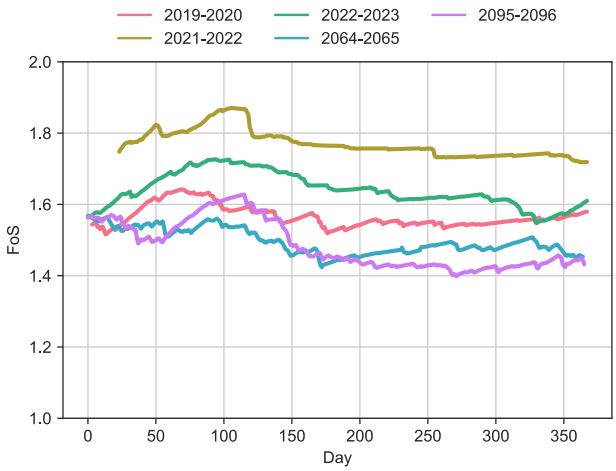

Fig. 5. *FoS* trends for the 5 different 1-year datasets.

The ten features used to train the models consisted of *P*, VWC at six different depths, PWP at 6 m depth, *T*, *LAI*. While the hydrological variables (i.e., VWC and PWP) for the past datasets are obtained from sensors installed on-site, this data is not available for the future datasets. Therefore, the values of VWC and PWP modelled using GeoStudio for future scenarios are used in the future datasets, as listed in Table 2. The target was the modelled *FoS* values obtained from the coupled use of transient SEEP/W and Slope modules (see Section 4.1).

Three specific groups, named as Group 1, Group 2, and Group 3, were thoughtfully created. The data from four 1-year datasets were used to train and test the data-driven model, and an independent dataset corresponding to the remaining fifth 1-year dataset was used for validation (Table 3). During the analysis, each 1-year dataset was separately considered for validation, and three selected groups are presented in the article. The Groups were first used to find the mutual correlations between the variables considered. The correlation check revealed that *P* has the weakest correlation with *FoS* values, and hence it was removed from the set of predictors for further analysis.

The validation was carried out as a two-step process for the data-driven approaches. For each Group, the training and testing datasets (Table 3) were split into two parts, 80 % for training and 20 % for testing. The training of the models was carried out using a 10-fold cross validation (Fabian Pedregosa et al., 2011) with mutual exclusion. The trained model was first tested on a part of the same Group dataset, and further tested on a validation dataset, i.e., different 1-year dataset (Table 3). The predictors in the training dataset were normalised using a standard scaler, and the same scaler was used to both normalise the test and validation datasets. The performance of the model has been evaluated comparing the forecasted *FoS*, using the data-driven approach, and the modelled *FoS* values, for GeoStudio, for the test and validation datasets, using the coefficient of determination (R^2) and, Root Mean Squared Error (*RMSE*)(Eq.(2) and (3)).

Table 3
Training and validation data used for finding the best-suited dataset for *FoS* forecast.

	Group 1	Group 2	Group 3
Training and testing datasets	2019–2020 2021–2022 2022–2023 2095–2096	2019–2020 2021–2022 2064–2065 2095–2096	2019–2020 2021–2022 2064–2065 2022–2023
Validation datasets	2064–2065	2022–2023	2095–2096

$$R^2 = 1 - \frac{\sum (y_i - \hat{y}_i)^2}{\sum (y_i - \bar{y})^2} \quad (2)$$

$$RMSE = \sqrt{\frac{\sum (y_i - \hat{y}_i)^2}{n}} \quad (3)$$

where y_i is the observed value, $\hat{y}_i$ is the forecasted value and $\bar{y}$ is the mean of the n observed values.

The first approach used a PR to fit the input data allowing for a flexible modelling of non-linear relationships. Three different degrees (i.e., 1,2,3) have been used to train the data of the three Groups (Table 3). Higher-degree polynomials have been neglected since can fit the training data more closely but may also be more prone to capturing noise and causing overfitting. The degree of PR was manually optimised after a trial-and-error approach. For Group 1 and Group 3 a PR model of degree two was the best in training and testing the datasets, while degree 1 has been selected for Group 2. The forecasted *FoS* values agree well with the modelled ones of the test dataset, with an R^2 values greater than 0.925 for all the three Groups considered (Table 4). As expected, the validation dataset displayed poorer performance metrics than the test ones, with Group 3 leading to the most favourable results, characterized by an R^2 value of 0.910 and an *RMSE* of 0.020.

The second method applies a RF algorithm (Ho, 1995) to forecast the *FoS* values using the explanatory variables. RF is an ensemble method that builds multiple decision trees using random subsets of data and features, combining their forecasts for improved accuracy and robustness in regression problems. RF solves a regression problem by constructing multiple decision trees on randomly sampled subsets of the training data, and then, averaging the forecasts of these trees. In this study, the hyper-parameters were also optimised at this stage using a grid-search cross-validation algorithm (Fabian Pedregosa et al., 2011). The algorithm optimises the values of hyper-parameters, from a given set of parameters in a grid. The number of trees in the forest, maximum number of levels in each decision tree and the minimum number of data points placed in a node before the node is split were optimised for each group separately, during the cross-validation process. The uncertainties in the forecasted values were estimated with a 95 % confidence interval, using the distribution of *FoS* values forecasted by all the decision trees in RF. The forecasted *FoS* values agree well with the modelled ones of the test dataset, with an R^2 values greater than 0.97 for all the three Groups considered (Table 4). The test datasets exhibited notably low *RMSE* values, with Group 2 having the smallest *RMSE* value at 0.005. As expected, the validation dataset displayed poorer performance metrics than the test datasets, with Group 1 yielding the most favourable outcomes, characterized by an R^2 value of 0.828 and an *RMSE* of 0.015. Notably, Group 2 exhibited suboptimal results in the validation dataset.

A detailed examination of the test and validation results for PR (Fig. 6a and b,c), showed that forecasts derived from the validation dataset of Group 2 exhibit substantial overestimation of *FoS* values. Group 1 and Group 3 showed good validation results with the second having a higher R^2 (0.910) and low *RMSE* (0.020). For this reason, the PR model trained with Group 3 has been chosen for forecasting analyses.

Table 4
Performance evaluation of data-driven *FoS* forecasts. In bold the best result for each model.

Data-driven model	Dataset	Test		Validation	
		R^2	*RMSE*	R^2	*RMSE*
PR	Group 1	0.973	0.018	0.770	0.018
	Group 2	0.925	0.031	−3.280	0.116
	Group 3	0.966	0.018	**0.910**	**0.020**
RF	Group 1	0.975	0.016	**0.828**	**0.015**
	Group 2	0.999	0.004	0.135	0.052
	Group 3	0.978	0.014	0.782	0.032

Upon detailed examination of the test and validation results for RF (Fig. 6d and e,f), the forecasted *FoS* values of Group 2 showed a nearly constant trend within a specific range of modelled *FoS* values between 1.6 and 1.7. Similarly, the validation dataset of Group 3 revealed a systematic underestimation of *FoS* values when the modelled values exceed 1.5, along with a quite flat trend, and overestimation when the modelled values fall below 1.45. Considering these observations and the associated performance metrics, the RF model trained using Group 1 were selected for *FoS* forecast within the digital twin.

While the *FoS* values of 2019–2020, 2064–2065 and 2095–2096 vary between 1.4 and 1.65, the *FoS* values of 2021–2022, were higher, ranging between 1.7 and 1.9 (Fig. 5). The dataset of 2022–2023 bridges this gap, and the results are better when this dataset is used for training, providing a continuous range of values varying between 1.4 and 1.9 for training. Both Groups 1 and 3 offers a wider and continuous range for all parameters, and therefore are more suitable to train data-driven models.

The scalers and the trained PR and RF models were stored as pickle files to facilitate the use within the cloud based LEWS framework. These pre-trained models, coupled with real-time input of forecasted meteorological and hydrological variables enabled dynamic and accurate forecasts of *FoS* for this case study.

5. Hydrological variables forecasting with pastas

The explanatory variables used for training the PR and the RF models and for forecasting *FoS* included meteorological (i.e., P, T) and hydrological variables (i.e., VWCs and PWP) as well as vegetation indicators (i.e., *LAI*). However, forecasts for hydrological variables (i.e., PWP and VWC) are not directly available, and they need to be carried out using as inputs the historical data and forecasted meteorological variables. To solve this issue and make a forecast of the VWC and PWP, a python-based package called Pastas (Collenteur et al., 2019) has been used. Pastas is an open-source Python package for the analysis of hydrogeological time series. It uses Transfer function noise (TFN) modelling to explain an observed time series (in this case monitored VWC and PWP) by one or more other observed time series. The observed VWC and PWP time series have been decomposed into the contributions of the different hydrological/meteorological variables (or stresses according to Collenteur et al., 2019), that cause the fluctuations. The use of stress models allows the incorporation of the influence of environmental factors on the observed time series, providing a comprehensive understanding of the temporal dynamics and interactions within the system. All the time dependent input variables used in GeoStudio (Table 2) are used as stress models in Pastas. The constant variables, *RD* and *VH* are not considered, as they are less influential in understanding the fluctuation of the hydrological variables. The VWC and PWP responses are simulated considering the stresses of measured and forecasted *P*, *T*, *SoR*, *RH*, *WS*, *SD*, *LAI* and albedo through the convolution (Collenteur et al., 2019):

$$h_m(t) = \int_{-\infty}^{t} S_m(\tau)\theta_m(t-\tau)d\tau$$

where S_m is a time series of stress m, and θ_m is the impulse response function for stress m. A commonly used impulse response function is the scaled Gamma distribution (Besbes and De Marsily, 1984).

Among all the stress, the historical values of *RH* are calculated using air temperature and dew point temperature, as given by Eq. (4), where e_s is the saturation vapor pressure at T and e_a is the actual vapor pressure at T_d, given by Eq. (5) and Eq. (6) respectively. While forecasted values of *RH* are obtained from Locationforecast API.

$$RH = \left(\frac{e_s}{e_a}\right) \times 100 \quad (4)$$

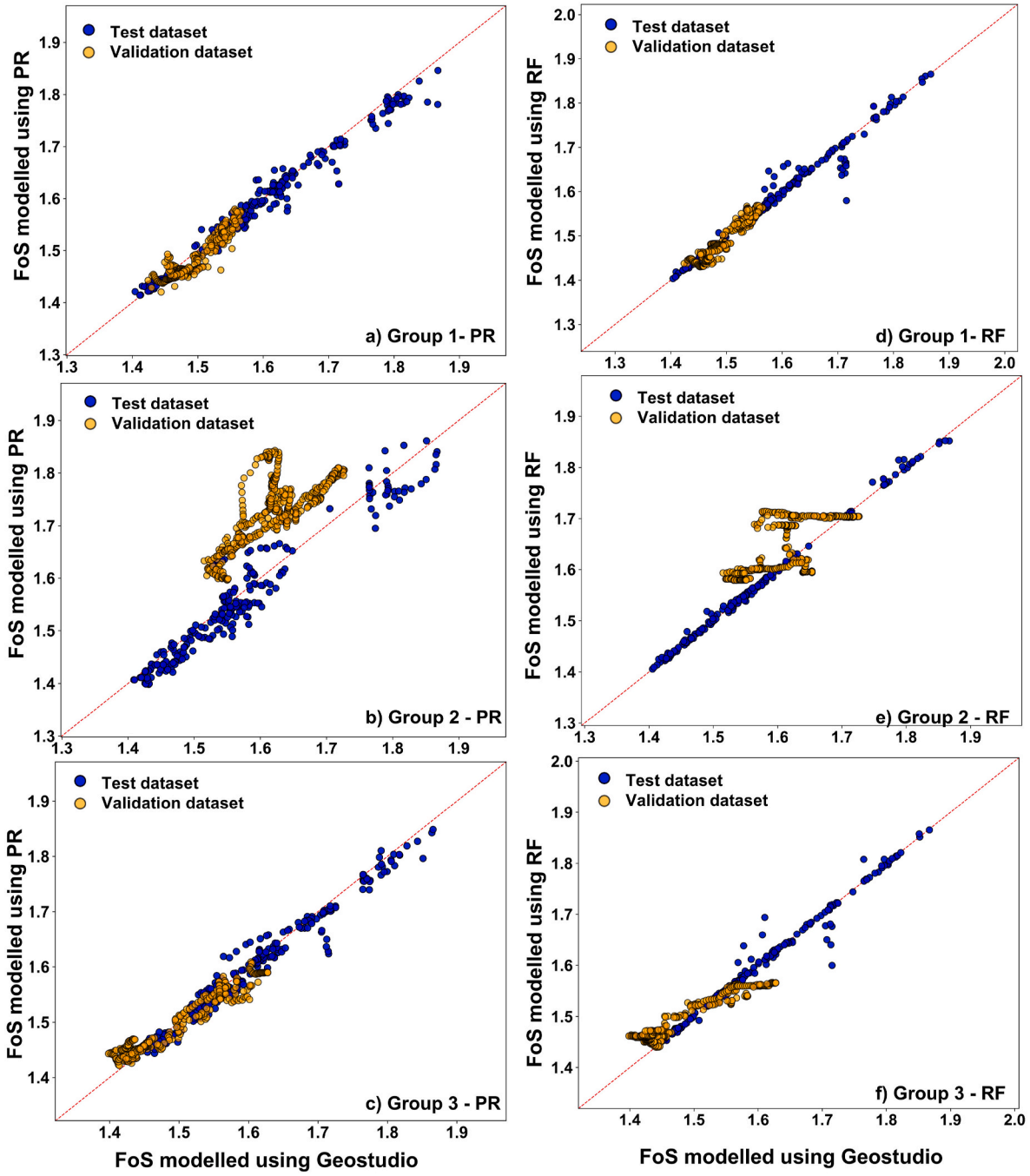

Fig. 6. *FoS* values modelled using GeoStudio vs data-driven models. a-c) results of PR and d-f) results of RF.

$$e_s = 6.122\left(e^{\left(\frac{17.67\times T}{T+243.5}\right)}\right) \quad (5)$$

$$e_a = 6.122\left(e^{\left(\frac{17.67\times T_d}{T_d+243.5}\right)}\right) \quad (6)$$

As an example, the variation of all the eight explanatory variables (or stresses) for the considered runtime day of the February 21, 2024 is plotted in Fig. 7. The figure contains daily historical data and forecasts up to the 24th of February. The trends of hydrological variables from the Pastas results are compared with the monitored data using the R^2 and *RMSE* metrics (Fig. 8).

The observed performance metrics vary across runs, demonstrating that Pastas effectively simulates hydrological variables, yielding R^2 values exceeding 0.79 for all variables. The best results were obtained for VWC and PWP at 6 m depth, with an R^2 of 0.99, while less favourable results were observed for the VWC at 0.1 m with R^2 value of 0.79. The *RMSE* were also satisfactory for all the cases. The metrics will be different for each run though, but large variations from the real time monitoring data have not been observed so far. The hydrological variables forecasted by Pastas were used as inputs in the PR and RF models for *FoS* forecasts.

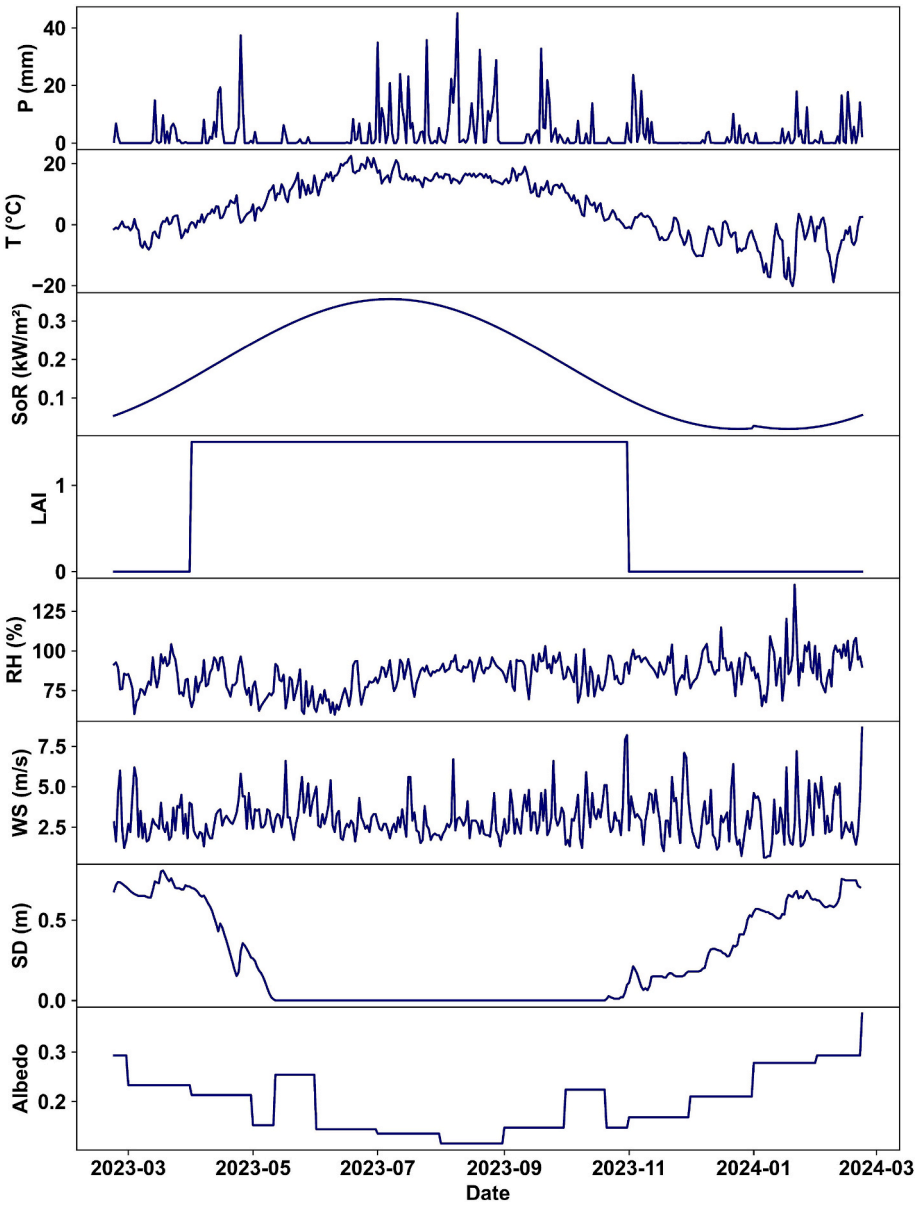

Fig. 7. Example of input variables for pastas.

6. Visualization of the forecasted hydrological variables and of the factor of safety

The final step of the proposed operational Lo-LEWS is to provide a simple and user-friendly dashboard for easy interpretation of the forecasted values. While *FoS* values are inherently understandable, the significance of VWC and PWP values for early warning purposes gain significance when they are contextualized against historical measurements taken at corresponding locations and depths. The substantial variability of these values, driven by soil characteristics, meteorological conditions, and vegetation variables, highlights the utility of normalised values over absolute values. The forecasted values are showed using a radar plot for hydrological variables (Fig. 9), ($x_{d,sc}$), normalised using Eq. (7).

$$x_{d,sc} = \frac{x_d - x_{min,n}}{x_{\max,n} - x_{min,n}} \tag{7}$$

where x_d is the forecasted value of a variable (VWC or PWP), and $x_{\max,n}$ and $x_{min,n}$ are the maximum and minimum values of the same variable, measured in the past n days, and the value of n is 365 in this study. This allows users to quickly understand the significance of hydrological variables, where values close to 1 indicates the proximity to the highest observed value in the past year, and values approaching zero indicate the opposite. Values outside the range [0,1] are also possible when the forecasted values are, respectively, lower or higher than the max and min values ever recorded in the past 365 days.

To show the forecasted values of *FoS*, a gauge plot has been used. Every gauge corresponds to 1-day forecast (Fig. 9b and c). Values approaching 1 are coloured in red and values higher than 2.5 are coloured in green. When the *FoS* is lower than 1.5 or the hydrological values are approaching 1, text messages and emails are sent to the system mangers to inform and, possibly, enable them to take action.

The dashboard also has time series plots of all the forecasted variables, enabling the users to understand the variations with respect to time (the link to video examples is available in the section Software and data availability). The forecasted hydrological variables are plotted along with the real-time measurements from the sensors, providing an option for easy comparison. Any significant variations in the forecasted values can thus be easily noted, and quality checks can be conducted in

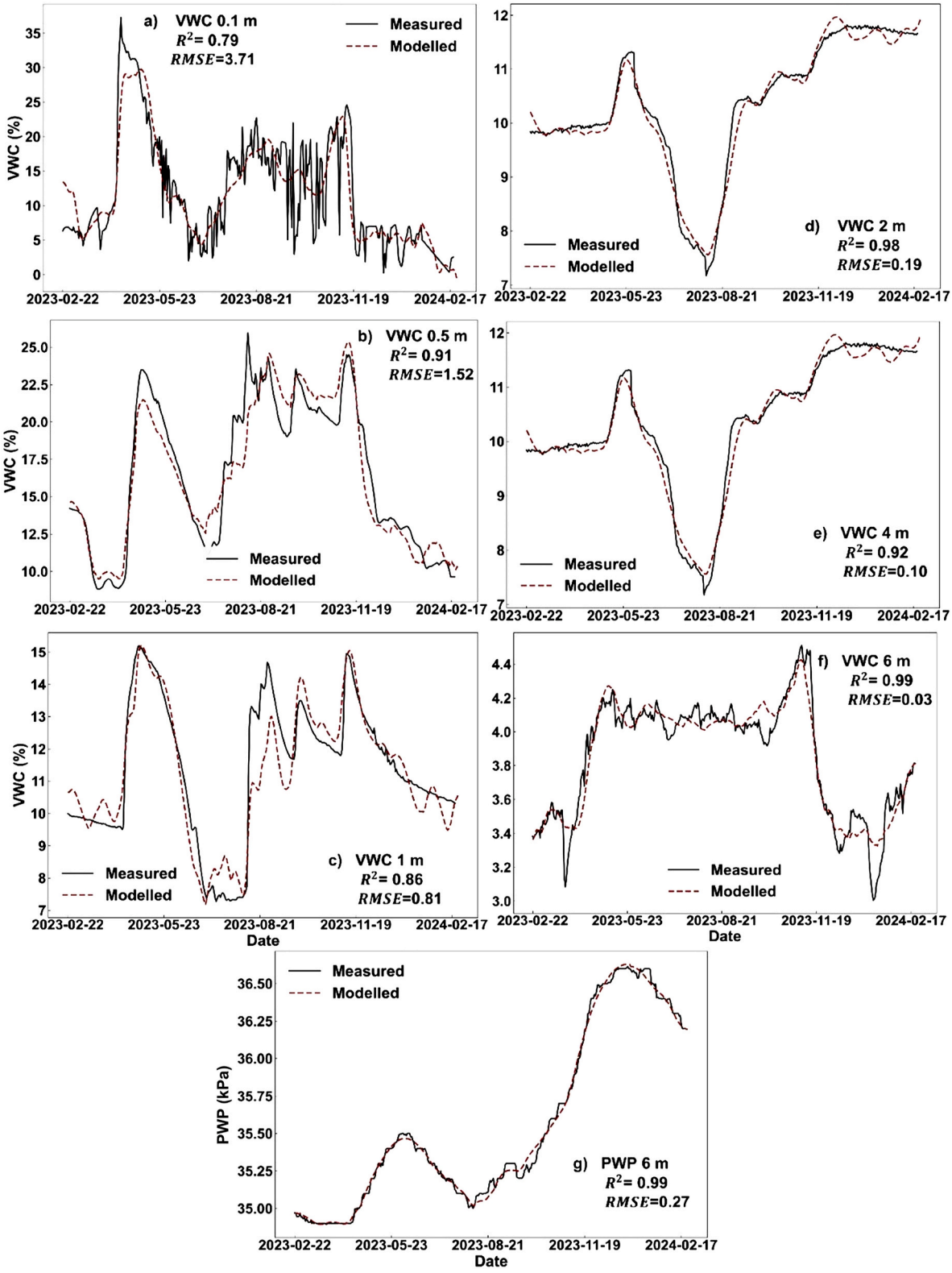

Fig. 8. Measured and modelled values of VWC and PWP using Pastas. A) VWC 0.1 m, b) VWC 0.5 m, c) VWC 1 m, d) VWC 2 m, e) VWC 4 m, f) VWC 6 m and g) PWP 6 m.

case of a discrepancy.

7. Discussion

Unlike common practices available in literature that rely on empirically derived threshold values for forecasting potential instability of initial landslides, and on displacement monitoring for slow moving landslide; the approach proposed in this paper fundamentally differs as the stability forecasts are completely based on hydrological and meteorological conditions.

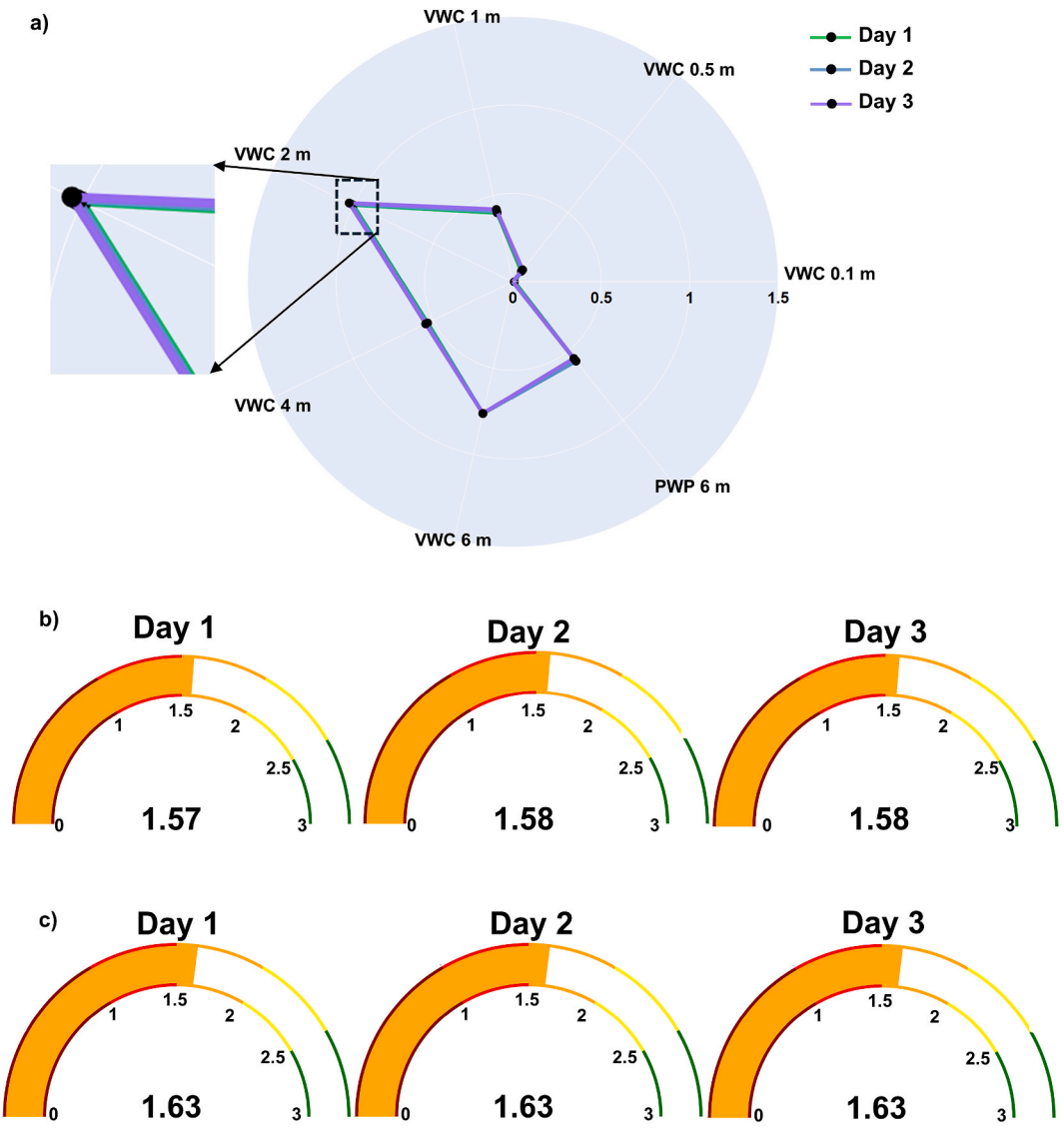

Fig. 9. Examples of output panels of the forecasted values of a) hydrological variables, b) *FoS* forecasted using PR and c) *FoS* forecasted using RF.

This paper introduces a digital twin model of the slope suitable for Lo-LEWS. The digital representation of the slope replicates its hydrological behaviour as a function of vegetation and meteorological dynamic inputs. It consists of a numerical model, the Pastas package and data-driven models. The approach relies on time-series monitoring data from field-installed sensors and publicly available meteorological data, data-driven models trained using a validated numerical model, and predictions of the hydrological behaviour of the slope. These components work together to predict the *FoS* of the slope. This study presents a completely operational workflow for such methods where data-driven models are used as proxies for physics-based models employed in WBPs in real-time.

The numerical model effectively back-calculates the hydrological behaviour of the slope up to one year. However, validation should occur every six months, as recommended by Piciullo et al., 2022. The validation involves running the numerical model for a six-month period and comparing the modelled hydrological variables (i.e., *VWC* and *PWP*) with the measured ones. Additionally, the hydrological variables forecasted with Pastas require ongoing validation too. In this regard, the user dashboard facilitates this process by plotting both monitored and forecasted hydrological variables on the same graph (the link to video examples is available in the section Software and data availability). This allows system managers to conduct a daily quality check of the forecasts made with Pastas. In case of significant discrepancies, a thorough examination of Pastas inputs and a revaluation of different hydrological and climate stresses are recommended. Another important aspect to consider is the performance evaluation of the PR and RF models in forecasting *FoS*. This can be achieved by comparing the forecasted *FoS* values with the ones obtained by running the numerical model in parallel.

Concerning the *FoS* forecast carried out with the data-driven models, it does not account for many uncertainties involved in the process. For instance, the RF algorithm is trained using a *FoS* range of 1.4–1.9. Although this range is relatively broad and it comes from the numerical modelling results, it does not extend below 1.4. This limitation poses challenges in forecasting *FoS* for lower values, which are the most critical ones. To mitigate this issue a PR model has also been used, in parallel, to forecast the *FoS*. The results are also plotted in the dashboard for comparison (the link to video examples is available in the section Software and data availability). PR model has the potential to extend forecasts beyond the range of observed data. However, it is essential to exercise caution when extrapolating, as the accuracy and reliability of forecasts may decrease as moving further away from the observed data range. This issue is clearly visible in Group 2 validation (Fig. 6), where

the model is trained with a visible gap in the *FoS* values, leading to a mismatch between *FoS* values modelled with GeoStudio and the data-driven models. A potential enhancement for future iterations could be incorporating a range of different extreme input values for the meteorological variables with the aim of having lower *FoS*, extending the *FoS* range. The model can be updated annually by adding the previous year's data to the training dataset.

Further, this approach can be used for Te-LEWS, using physics-based or data-driven approaches. The architecture and the digital infrastructure require several changes to develop such an operational slope stability forecast in a regional scale. While the slope scale model forecasts a single value of *FoS*, the output for a territorial scale model for each timestep is a map layer consisting of spatially varying *FoS* values, or probability of occurrence of landslides. This can be done either using physics-based models or data-driven models. For a physics-based model, precise subsurface data is critical along with the landslide database and the meteorological parameters, while data-driven models can be developed using landslide conditioning factors, triggering factors, and their historical relationship with the occurrence of landslides. This work marks the beginning of an attempt to develop reproducible and automated workflows which can be used in Lo and Te-LEWS.

8. Conclusions

This paper provides a significant contribution is the development of a fully automatic IoT procedure for real-time slope stability forecast built upon the framework proposed by Piciullo et al., 2022. It is designed on four key technical aspects: monitoring, modelling, forecasting and warning, for slopes that have not shown any prior deformations. The paper explores an integrated approach, combining real-time hydrological monitoring, meteorological data, and numerical modelling results to use in data-driven models for slope stability forecasting. The models have been used to compute the *FoS* for 5 different 1-year datasets. Historical and future hydrological, meteorological and vegetation variables have been used as inputs. The inclusion of both historical and future data enhances the robustness of the models. These inputs and the *FoS* results of the 5 datasets have been grouped in 3 Groups and used to train the data-driven models.

This paper describes a first-time attempt to develop a IoT-based real-time Lo-LEWS, using hydrological and vegetation indicators along with the conventional meteorological and field monitoring data. The proposed approach was successfully implemented for a slope in Norway, the results are plotted using a web-based platform, which shows the forecasted *FoS* values of the slope for the rolling three days. The stability is evaluated based on historical and forecasted hydrological, meteorological and vegetation conditions. The study demonstrates the need of an interdisciplinary approach across diverse expertise areas, including geotechnics, hydrology, meteorology, instrumentation, and informatics, in developing an IoT-based real-time Lo-LEWS. Moreover, the paper also highlights the possibility of forecasting the slope stability using hydrological variables. This was achieved using a numerical model of the slope using GeoStudio, along with Pastas package and data-driven models which define a digital twin of the slope, enabling real-time *FoS* forecasts. This innovative approach enhances the understanding and monitoring capabilities of the slope, and it can be useful for those slopes that have not shown any previous deformations, but that still pose a threat to elements exposed.

The success of this framework is attributed to a collaborative effort across diverse expertise areas, including geotechnics, hydrology, meteorology, instrumentation, and informatics. In essence, the study presents a holistic and groundbreaking approach to slope stability forecasting, utilizing cutting-edge technologies and interdisciplinary collaboration. Moreover, the framework developed can also be extended to the regional scale for the development of IoT-based real-time Te-LEWS.

Software and data availability

The code for the slope stability digital twin used in the study is publicly available on GitHub. Credentials are required to interact with the NGI Live real-time data platform and the APIs from the Norwegian Meteorological Institute and the Open-Meteo. Cloud infrastructure for Azure Function deployment is set up separately.

Developer: Norwegian Geotechnical Institute (NGI).

Contact: Dr. Luca Piciullo - luca.piciullo@ngi.no.

Year first available: 2024.

Code availability: https://github.com/norwegian-geotechnical-institute/local-slope-stability-forecast.

License: MIT.

Programming language: python.

Dependencies: see dependency files in git repository.

Operating system: Linux or Windows.

Data availability: Historical and forecast meteorological data used in the analyses are fetched from the APIs links provided in the paper. Authentication for the NGI Live data API is not available publicly.

The data used to train the data-driven models are available here:
https://sapubslopestabilityprod.blob.core.windows.net/data/2019_2020.csv
https://sapubslopestabilityprod.blob.core.windows.net/data/2021_2022.csv
https://sapubslopestabilityprod.blob.core.windows.net/data/2022_2023.csv
https://sapubslopestabilityprod.blob.core.windows.net/data/2064_2065.csv
https://sapubslopestabilityprod.blob.core.windows.net/data/2095_2096.csv.

Moreover, it is important to underline that our workflow is fully automated and fetches data and publish results to NGI Live in real time without storing the input data.

The reader can find videos showcasing the dashboard in the GitHub folder: https://github.com/norwegian-geotechnical-institute/local-slope-stability-forecast/tree/trunk/videos.

CRediT authorship contribution statement

Luca Piciullo: Writing – review & editing, Writing – original draft, Project administration, Methodology, Data curation, Conceptualization. **Minu Treesa Abraham:** Writing – review & editing, Writing – original draft, Visualization, Validation, Software, Formal analysis. **Ida Norderhaug Drøsdal:** Writing – review & editing, Software, Conceptualization. **Erling Singstad Paulsen:** Writing – review & editing, Visualization, Data curation.

Declaration of competing interest

The authors declare that they have no known competing financial interests or personal relationships that could have appeared to influence the work reported in this paper.

Data availability

GitHub repository has been created with data and codes

Acknowledgment

The authors want to express sincere gratitude to Margherita Pavanello for her valuable contribution to the creation of Fig. 1 in this scientific paper. Additionally, the authors thank Emir Ahmet Oguz for providing the script to retrieve meteorological forecast data from the Norwegian Meteorological Institute. Finally, the authors gratefully acknowledge the support received from the basic funding to NGI from The Research Council of Norway and the HuT EU project (ID101073957,

https://thehut-nexus.eu/), which played a crucial role in facilitating and advancing our research.

References

Abraham, M.T., Satyam, N., Pradhan, B., Alamri, A.M., 2020. Iot-based geotechnical monitoring of unstable slopes for landslide early warning in the Darjeeling Himalayas. Sensors 20. https://doi.org/10.3390/s20092611.

Abraham, M.T., Satyam, N., Pradhan, B., Segoni, S., Alamri, A., 2022. Developing a prototype landslide early warning system for Darjeeling Himalayas using SIGMA model and real-time field monitoring. Geosci. J. 26, 289–301. https://doi.org/10.1007/s12303-021-0026-2.

Bell, R., 2010. Integrative Frühwarnsysteme für gravitative Massenbewegungen (ILEWS): Monitoring, 1974-. Modellierung, Implementierung. Klartext.

Besbes, M., De Marsily, G., 1984. From infiltration to recharge: use of a parametric transfer function. J. Hydrol. (Amst.) 74, 271–293. https://doi.org/10.1016/0022-1694(84)90019-2.

Bossi, G., Schenato, L., Marcato, G., 2023. Web-based platforms for landslide risk mitigation: the state of the art. Water 15, 1632. https://doi.org/10.3390/w15081632, 2023.

Calvello, M., 2017. Early warning strategies to cope with landslide risk. Riv. Ital. Geotec. 51, 63–91. https://doi.org/10.19199/2017.2.0557-1405.063.

Calvello, Michele, d'Orsi, R.N., Piciullo, L., Paes, N., Magalhaes, M., Lacerda, W.A., 2015. The Rio de Janeiro early warning system for rainfall-induced landslides: analysis of performance for the years 2010–2013. Int. J. Disaster Risk Reduc. 12, 3–15. https://doi.org/10.1016/j.ijdrr.2014.10.005.

Calvello, M., D'Orsi, R.N., Piciullo, L., Paes, N.M., Magalhaes, M.A., Coelho, R., Lacerda, W.A., 2015. The community-based alert and alarm system for rainfall induced landslides in Rio de Janeiro, Brazil. Engineering Geology for Society and Territory 2. https://doi.org/10.1007/978-3-319-09057-3_109. Landslide Processes.

Capobianco, V., Robinson, K., Kalsnes, B., Ekeheien, C., Høydal, Ø., 2021. Hydro-mechanical effects of several riparian vegetation combinations on the streambank stability — a benchmark case in southeastern Norway. Sustainability 13. https://doi.org/10.3390/su13074046.

Charléty, A., Le Breton, M., Baillet, L., Larose, E., 2023. RFID landslide monitoring: long-term outdoor signal processing and phase unwrapping. IEEE Journal of Radio Frequency Identification 7, 319–329. https://doi.org/10.1109/JRFID.2023.3256560.

Cherubini, F., Vezhapparambu, S., Bogren, W., Astrup, R., Strømman, A.H., 2017. Spatial, seasonal, and topographical patterns of surface albedo in Norwegian forests and cropland. Int J Remote Sens 38, 4565–4586. https://doi.org/10.1080/01431161.2017.1320442.

Collenteur, R.A., Bakker, M., Caljé, R., Klop, S.A., Schaars, F., 2019. Pastas: open source software for the analysis of groundwater time series. Groundwater 57, 877–885. https://doi.org/10.1111/gwat.12925.

Cruden, D.M., Varnes, D.J., 1996. Landslide Types and Processes. Transportation Research Board.

Dahlberg, U., Berge, T.W., Petersson, H., Vencatasawmy, C.P., 2004. Modelling biomass and Leaf area Index in a sub-arctic scandinavian mountain area. Scand. J. For. Res. 19, 60–71. https://doi.org/10.1080/02827580310019266.

El Houssaini, D., Khriji, S., Viehweger, C., Keutel, T., Kanoun, O., 2022. Location-aware IoT-enabled wireless sensor networks for landslide early warning. Electronics (Switzerland) 11. https://doi.org/10.3390/electronics11233971.

Dibiagio, E., Kjekstad, O., 2007. Day3-Session5 2 Nd Regional Training Course (RECLAIM Phase II) Early Warning, Instrumentation and Monitoring Landslides.

Fathani, T.F., Karnawati, D., Wilopo, W., n.d. An integrated methodology to develop a standard for landslide early warning system. https://doi.org/10.5194/nhess-2016-209.

Gamperl, M., Singer, J., Thuro, K., 2021. Internet of things geosensor network for cost-effective landslide early warning systems. Sensors 21. https://doi.org/10.3390/s21082609.

Gian, Q.A., Tran, D.T., Nguyen, D.C., Nhu, V.H., Tien Bui, D., 2017. Design and implementation of site-specific rainfall-induced landslide early warning and monitoring system: a case study at Nam Dan landslide (Vietnam). Geomatics, Nat. Hazards Risk 8, 1978–1996. https://doi.org/10.1080/19475705.2017.1401561.

Guzzetti, F., Gariano, S.L., Peruccacci, S., Brunetti, M.T., Marchesini, I., Rossi, M., Melillo, M., 2020. Geographical landslide early warning systems. Earth Sci. Rev. https://doi.org/10.1016/j.earscirev.2019.102973.

Hanssen-Bauer, I., Førland, E.J., Haddeland, I., Hisdal, H., Lawrence, D., Mayer, S., Nesje, A., Nilsen, J.E.Ø., Sandven, S., Sandø, A.B., Sorteberg, A., Ådlandsvik, B., n.d. Climate in Norway 2100 Lead Authors-A Knowledge Base for Climate Adaptation.

Heyerdahl, H., Høydal, Ø.A., Gisnås, G., Kvistedal, Y., Carotenuto, P., 2018. 2018_Heyerdahl et al._slope instrumentation and unsaturated stability. In: 7th International Conference on Unsaturated Soils 2018 (Hong Kong).

Ho, T.K., 1995. Random decision forests. In: Proceedings of the International Conference on Document Analysis and Recognition, ICDAR, pp. 278–282. https://doi.org/10.1109/ICDAR.1995.598994.

Hungr, O., Leroueil, S., Picarelli, L., 2014. The Varnes classification of landslide types, an update. Landslides 11, 167–194. https://doi.org/10.1007/s10346-013-0436-y.

Intrieri, E., Gigli, G., Casagli, N., Nadim, F., 2013. Brief communication landslide early warning system: toolbox and general concepts. Natural Hazards and Earth System Science 13, 85–90. https://doi.org/10.5194/nhess-13-85-2013.

Jaedicke, C., Kleven, A., 2008. Long-term precipitation and slide activity in south-eastern Norway, autumn 2000. Hydrol. Process. 22, 495–505. https://doi.org/10.1002/hyp.6878.

Ju, N. pan, Huang, J., Huang, R. qiu, He, C. yang, Li, Y. rong, 2015. A Real-time monitoring and early warning system for landslides in Southwest China. J. Mt. Sci. 12, 1219–1228. https://doi.org/10.1007/s11629-014-3307-7.

Kim, K.S., Jeong, S.W., Song, Y.S., Kim, M., Park, J.Y., 2021. Four-year monitoring study of shallow landslide hazards based on hydrological measurements in a weathered granite soil slope in South Korea. Water (Switzerland) 13. https://doi.org/10.3390/w13172330.

Kotta, H.Z., Rantelobo, K., Tena, S., Klau, G., 2011. Wireless sensor network for landslide monitoring in nusa tenggara timur. TELKOMNIKA 9, 9–18.

Kuradusenge, M., Kumaran, S., Zennaro, M., Niyonzima, A., 2021. Experimental study of site-specific soil water content and rainfall inducing shallow landslides: case of gakenke district, Rwanda. Geofluids. https://doi.org/10.1155/2021/7194988, 2021.

Lussana, C., Saloranta, T., Skaugen, T., Magnusson, J., Tveito, O.E., Anderson, J., 2018. seNorge2 daily precipitation, an observational gridded dataset over Norway from 1957 to the present day. Earth Syst. Sci. Data 10, 235–249. https://doi.org/10.5194/essd-10-235-2018.

Marino, P., Roman Quintero, D.C., Santonastaso, G.F., Greco, R., 2023. Prototype of an IoT-based low-cost sensor network for the hydrological monitoring of landslide-prone areas. Sensors 23. https://doi.org/10.3390/s23042299.

Mirus, B.B., Becker, R.E., Baum, R.L., Smith, J.B., 2018. Integrating real-time subsurface hydrologic monitoring with empirical rainfall thresholds to improve landslide early warning. Landslides 15, 1909–1919. https://doi.org/10.1007/s10346-018-0995-z.

Oguz, E.A., Depina, I., Myhre, B., Devoli, G., Rustad, H., Thakur, V., 2022. IoT-based hydrological monitoring of water-induced landslides: a case study in central Norway. Bull. Eng. Geol. Environ. 81. https://doi.org/10.1007/s10064-022-02721-z.

Park, S., Lim, H., Tamang, B., Jin, J., Lee, S., Chang, S., Kim, Y., 2019. A study on the slope failure monitoring of a model slope by the application of a displacement sensor. J. Sens. https://doi.org/10.1155/2019/7570517, 2019.

Pecoraro, G., Calvello, M., Piciullo, L., 2019. Monitoring strategies for local landslide early warning systems. Landslides 16. https://doi.org/10.1007/s10346-018-1068-z.

Pedregosa, Fabian, Varoquaux, Gaël, Gramfort, Alexandre, Vincent, Michel, Bertrand, Thirion, Grisel, Olivier, Blondel, Mathieu, Müller, Andreas, Nothman, Joel, Louppe, Gilles, Prettenhofer, Peter, Weiss, Ron, 2011. Scikit-learn: machine learning in Python. J. Mach. Learn. Res. 12, 2825–2830.

Piciullo, L., Calvello, M., Cepeda, J.M., 2018. Territorial early warning systems for rainfall-induced landslides. Earth Sci. Rev. 179. https://doi.org/10.1016/j.earscirev.2018.02.013.

Piciullo, L., Capobianco, V., Heyerdahl, H., 2022. A first step towards a IoT-based local early warning system for an unsaturated slope in Norway. Nat. Hazards 114. https://doi.org/10.1007/s11069-022-05524-3.

Sofwan, A., Sumardi, Ridho, M., Goni, A., Najib, 2017. Wireless sensor network design for landslide warning system in IoT architecture. In: 2017 4th International Conference on Information Technology, Computer, and Electrical Engineering (ICITACEE). IEEE, pp. 280–283. https://doi.org/10.1109/ICITACEE.2017.8257718.

Stähli, M., Sättele, M., Huggel, C., McArdell, B.W., Lehmann, P., Van Herwijnen, A., Berne, A., Schleiss, M., Ferrari, A., Kos, A., Or, D., Springman, S.M., 2015. Monitoring and prediction in early warning systems for rapid mass movements. Nat. Hazards Earth Syst. Sci. 15, 905–917. https://doi.org/10.5194/nhess-15-905-2015.

Sun, J., Li, H., Liu, Y., 2024. Data-driven early warning indicator for the overall stability of rock slopes: an example in hydropower engineering. Environ. Model. Software 175, 105994. https://doi.org/10.1016/j.envsoft.2024.105994.

Thiebes, B., Glade, T., 2016. Landslide Early Warning Systems—fundamental concepts and innovative applications. In: Landslides and Engineered Slopes. Experience, Theory and Practice. CRC Press, pp. 1903–1911. https://doi.org/10.1201/b21520-238.

Thiebes, B., Bell, R., Glade, T., 2012. Landslide analysis and integrative early warning – local and regional case studies. In: Eberhardt, E., Froese, C., Turner, K., Leroueil, S. (Eds.), Landslides and Engineered Slopes: Protecting Society ThroughImproved Understanding. CRC Press, Banff, Alberta, Canada.

Web references

ZL6 - METER Group, URL https://metergroup.com/products/zl6/(accessed 2.19.24).

ATMOS 41 - METER Group, URL https://metergroup.com/products/atmos-41/(accessed 2.19.24).

TEROS 12 - METER Group, URL https://metergroup.com/products/teros-12/(accessed 2.19.24).

TEROS 21 - METER Group, URL https://metergroup.com/products/teros-21/(accessed 2.19.24).

Data Loggers - Delta T, URL https://delta-t.co.uk/product-category/data-loggers/(accessed 2.19.24).

SM150T Soil Moisture Sensor - Soil Water content - Soil Humidity Sensor, URL https://delta-t.co.uk/product/sm150t/(accessed 2.19.24).

PVT Direct push piezometer with built-in data logger | GEOTECH, URL https://geotech.eu/product/pvt-direct-push-piezometer-with-built-in-data-logger/(accessed 2.19.24).

Azure Functions Overview | Microsoft Learn, URL https://learn.microsoft.com/en-us/azure/azure-functions/functions-overview?pivots=programming-language-csharp (accessed 2.19.24).

Timer trigger for Azure Functions | Microsoft Learn, URL https://learn.microsoft.com/en-us/azure/azure-functions/functions-bindings-timer?tabs=python-v2%2Cisolated-process%2Cnodejs-v4&pivots=programming-language-csharp (accessed 2.19.24).

Azure Monitor overview - Azure Monitor | Microsoft Learn, URL https://learn.microsoft.com/en-us/azure/azure-monitor/overview (accessed 2.19.24).
Azure Blob Storage | Microsoft Azure, URL https://azure.microsoft.com/en-us/products/storage/blobs (accessed 2.19.24).
Key Vault | Microsoft Azure, URL https://azure.microsoft.com/en-us/products/key-vault (accessed 2.19.24).
Frost API, 2024. MET Norway. https://frost.met.no/index.html.
Historical Weather API | Open-Meteo.com, URL https://open-meteo.com/en/docs/historical-weather-api (accessed 3.5.24).
MET Norway, 2024. Locationforecast 2.0. https://api.met.no/weatherapi/locationforecast/2.0/.
MET Norway API | Open-Meteo.com, URL https://open-meteo.com/en/docs/metno-api (accessed 3.5.24).
SeNorge - Se snøkart og klimakart for hele Norge, URL https://www.senorge.no/(accessed 2.19.24).
Forside - Norsk klimaservicesenter, URL https://klimaservicesenter.no/(accessed 2.19.24).